NONLINEAR VIBRATION OF AN EDGE-CRACKED BEAM WITH A COHESIVE ZONE, II: PERTURBATION ANALYSIS OF EULER-BERNOULLI BEAM VIBRATION USING A NONLINEAR SPRING FOR DAMAGE REPRESENTATION

Daniel A. Mendelsohn, Sridhar Vedachalam, Claudio Pecorari
and Prasad S. Mokashi

NONLINEAR VIBRATION OF AN EDGE-CRACKED BEAM WITH A COHESIVE ZONE, II: PERTURBATION ANALYSIS OF EULER-BERNOULLI BEAM VIBRATION USING A NONLINEAR SPRING FOR DAMAGE REPRESENTATION

DANIEL A. MENDELSOHN, SRIDHAR VEDACHALAM,
CLAUDIO PECORARI AND PRASAD S. MOKASHI

A nonlinear free-vibration analysis of an Euler–Bernoulli beam with an edge crack and a cohesive zone at the crack tip, represented by bending and shear springs, is presented. Restricting attention to bending nonlinearities, we suppose the beam is loaded statically in bending into the nonlinear region and small amplitude vibrations are then superposed. A two term perturbation expansion is used where the small parameter depends on the ratio of the first and second derivatives of the nonlinear moment-slope relations computed in Part I. The zeroth order term is the linear free-vibration solution (constant spring stiffness equal to the first derivative of the moment-slope relation). Each mode generates a second harmonic (first-order term) whose magnitude depends on the linear spring stiffness and on the small perturbation parameter. Key features of the zeroth and first-order solutions are studied as functions of the moment-slope relations computed in Part I, and the possibility of cohesive property characterization is discussed.

1. Introduction

Material characterization based on vibration characteristics is an important quantitative nondestructive evaluation (QNDE) tool. The presence of cracks in a structure causes an increase in structural and material compliance, reduction in the natural frequencies, and changes in the mode shapes. Natural frequency and mode shape versus crack geometry relationships are of interest, for example, in the assessment of the performance integrity of cracked structures, nondestructive evaluation of the extent and location of cracking, and prediction of the resonant frequency in high-cycle fatigue. The reduction in natural frequencies caused by transverse cracks in linear elastic beams and similar thin structures has been studied extensively both theoretically and experimentally. (See [Gudmundson 1982; Gudmundson 1983; Bamnios and Trochidis 1995a; Bamnios and Trochidis 1995b; Dimarogonas 1996; Chondros and Dimarogonas 1998; Gounaris and Papadopoulos 1997; Chondros et al. 1998; Yokoyama and Chen 1998; Shifrin and Ruotolo 1999; Mahmoud et al. 1999; Li 2001; Chondros 2001]. See also the numerous references in [Kessler et al. 2002], and the extensive review in [Dimarogonas 1996].) A typical beam analysis involves a linear elastic frequency analysis of the vibrating beam, modeled by Euler–Bernoulli or some higher order beam theory on either side of the (infinitesimally thin) crack plane along with one of various models for representing the localized increased compliance of the beam in the neighborhood of the crack plane caused by the presence of the crack. One such model, used in the present analysis and previously by Yokoyama and Chen [1998] and Mendelsohn [2006], is the line-spring model [Rice

and Levy 1972], which replaces the crack plane with shear and bending springs, whose stiffnesses are found from fracture mechanics solutions of edge-cracked geometries under appropriate loading. The analysis of Yokoyama and Chen [1998] assumes elastic behavior at the crack tip(s) which allows the spring constants to be found from well-tabulated elastic fracture mechanics solutions for stress intensity factors. In the absence of material nonlinearity, the spring constants found in this way are independent of load and depend only on crack length and specimen geometry.

The majority of the work cited above in vibration signatures of cracked structures has been linear and elastic and the only nonlinearity that has been studied is that due to intermittent crack face contact during a vibration cycle, known as the breathing crack phenomenon. This results in higher harmonics generated through the coupling of the bending vibrations with longitudinal motions in the direction of the opening and closing crack faces [Dimarogonas 1996; Chondros et al. 2001; Brandon et al. 1999; Sekhar and Balaji Prasad 1998; Ruotolo et al. 1996]. The reductions in natural frequencies compared to the uncracked beam are less than when the crack closure portions of the vibration cycle are prevented from occurring, say due to a static preload.

Turning to material types of nonlinearity, we note, as discussed in detail in the companion paper [Mokashi and Mendelsohn 2008], that many materials exhibit a region of cohesive behavior that is limited to a thin planar zone ahead of the crack tip, often referred to as a cohesive zone. The only beam vibration analysis that considers plastic or cohesive behavior at the crack tip that the authors are aware of is that of [Mendelsohn 2006], who also solves a free-vibration problem for the cracked beam using the line-spring model. However, despite the nonlinear behavior of the $M - \Delta\theta$ relationships found using a Dugdale–Barenblatt cohesive zone, the dynamic response is assumed to be linear and the stiffness constant is taken to be the slope of the nonlinear $M - \Delta\theta$ curve. In other words, at a given static preload M_S, the dynamic response is assumed to take place linearly along the local tangent to the nonlinear $M - \Delta\theta$ curve. Since the crack plane is taken at the midspan, and the applied static preload is in bending only, as will be the case in the present analysis as well, only the symmetric modes activate the bending cohesive behavior and the shear response is always elastic. The shear line-spring stiffness was therefore calculated as in [Yokoyama and Chen 1998] and confirmed by the BEM analysis in the doctoral thesis by Mokashi [2007]. For sufficiently large static preloads, the resulting linear eigenvalue problem results in markedly reduced natural frequencies compared to the elastic cracked case with no cohesive zones.

The present work extends that of Mendelsohn [2006] in two ways. First, it makes use of the nonlinear $M - \Delta\theta$ curves for the linear softening cohesive zone [Mokashi and Mendelsohn 2008], as opposed to those for Dugdale–Barenblatt cohesive zones. This is important for many materials, which exhibit softening behavior before crack growth and ultimate failure. And second, it is the first attempt to address the nonlinearity of the line-spring directly in the dynamic analysis. This is done by employing an asymptotic or perturbation technique used in nonlinear dynamics. The method involves identifying the nonlinear part of the nonlinear bending spring boundary condition, and writing it in such a way that it is multiplied by a parameter, which can be argued to be small. The solution is then expanded in powers of the small parameter, and by collecting terms of like powers of the small parameter, a series of linear boundary conditions are generated. The lowest order boundary conditions are naturally linear, while the nonlinear terms in the original formulation result in nonlinear combinations of lower order results appearing as known loading terms in the higher order linear problems. This method has been widely used for including weak nonlinearities throughout nonlinear dynamics; spatially discrete and

spatially continuous systems, and in the time domain and frequency domain. In problems similar to the present one, Pecorari [2003; 2004] and Pecorari and Pozníc [2005] have used a perturbation approach in a frequency domain analysis of wave transmission and reflection at contact interfaces, where the elasto-plastic contact is represented by nonlinear springs. The work presented here is a first step toward evaluating the feasibility of and developing an inverse technique, which would determine the cohesive law parameters from measurements of the nonlinear contributions to the dynamic response of edge-cracked beam specimens.

2. Nonlinear beam vibration formulation

In the following the line-spring model for a cracked beam is introduced, and the relationship between the quasistatic nonlinear bending deformation across the crack-plane and the nonlinear small amplitude dynamic response about a quasistatic preload is discussed. Since the present study is aimed at characterizing only cohesive nonlinearity effects, the well understood nonlinearity due to crack face contact is avoided by assuming a static preload for two reasons. While the contact conditions could be added, and the vibration problem without the static preload could be treated with a slightly modified perturbation method, that would (i) only confuse the issue at hand by mixing the two nonlinear effects, and (ii) require extremely large vibration amplitudes to activate significant cohesive behavior during a test. The latter would be almost impossible to control, so as is commonly done in QNDE, the cohesive zone is activated by the static preload and the superposed vibrations are assumed to be of small amplitude about this preload state.

The resulting nonlinear motions about the static preload are represented as a two-term series in a small parameter which depends on the quasistatic nonlinear bending deformation behavior and on the nondimensional amplitude of the free vibration response. This yields two uncoupled problems; one that is of zeroth order in the small parameter which is the fundamental modified free-vibration eigenvalue problem. The second of these problems (first order in the small parameter) is a forced vibration problem where the source term is the zeroth order contribution to the nonlinear bending spring boundary condition, which is solved for first from the zeroth order problem. For each natural frequency and mode shape from the zeroth order problem, there is a first-order solution with known amplitude and frequency twice that of the natural frequency (that is, the nonlinearity generates a complete set of second harmonics). Consider a simply supported Euler–Bernoulli beam of rectangular cross-section A, containing an edge-crack of length a located a distance c from the left end; see Figure 1. The beam has length L, depth W and thickness b ($A = b \cdot W$), although all measurable results are independent of the thickness b. The presence of the crack allows discontinuities in transverse deflection (Δv) and slope of the deflection ($\Delta \theta$) across the crack-plane [Mokashi and Mendelsohn 2008, Figure 1]. Recalling the line-spring model of the crack-plane presented in [Mokashi and Mendelsohn 2008], we rewrite the bending and shear interactions [Mokashi and Mendelsohn 2008, Equations (1) and (2)] in terms of resistance or stiffness rather than compliance.

$$M = R_N(\Delta\theta) \tag{1a}$$

$$Q = R_T(\Delta v) = K_T \Delta v. \tag{1b}$$
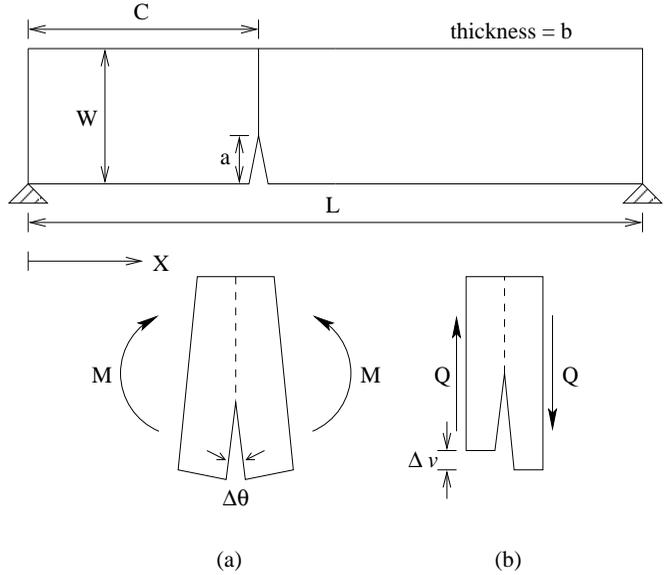
Figure 1. (a) Geometry of an edge-cracked beam. (b) Discontinuity in slope and deflection under mode I and mode II loading, respectively.

Here R represents the resistance to crack-plane deformation. If material behavior is linear for a particular mode, then that R is a linear function of the deformation with slope equal to the stiffness. Since the static preload and resulting cohesive behavior is in bending only, the shear spring is assumed linear throughout, and the second equality in Equation (1b) is used, where K_T is the stiffness obtained from an elastic mode II loading crack solution.

The nonlinearity in the bending spring is now treated. Consider a general nonlinear quasistatic softening relationship for the bending spring (Figure 2) representing any of the predicted relations from [Mokashi and Mendelsohn 2008, Figures 8 and 9]. In order to isolate the bending effects, the crack is placed in the middle of the beam ($c = L/2$) so that the odd modes excite only mode I deformations. Now assume a static mode I preload, represented by the point $[\Delta\theta_s, M_s]$ in Figure 2, and further assume that
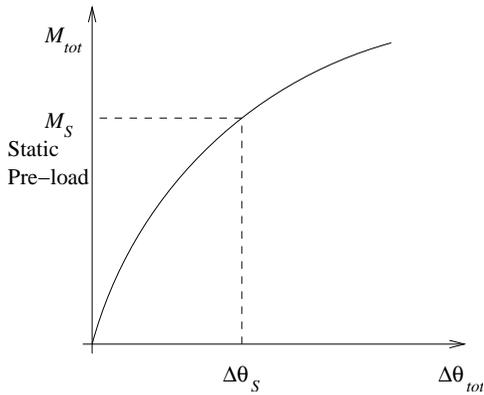
Figure 2. A generic nonlinear quasistatic $M - \Delta\theta$ curve.

small amplitude free vibrations occur about the preload state. Neglecting hysteresis, a first approximation for the dynamic behavior is that the point $[\theta_{\text{tot}}, M_{\text{tot}}]$ lies along the tangent to the curve at $[\Delta\theta_s, M_s]$ [Mendelsohn 2006] where 'tot' indicates the total response which is sum of the static and dynamic responses. This is equivalent to taking the total response to be the first two terms of a Taylor series expansion about $[\Delta\theta_s, M_s]$. This approximation is refined here by assuming that the dynamic response is nonlinear as well and that $[\theta_{\text{tot}}, M_{\text{tot}}]$ lies along a parabola at $[\Delta\theta_s, M_s]$, that is, the first three terms in the Taylor series about $[\Delta\theta_s, M_s]$:

$$M_{\text{tot}} = M_s + K_{N0}(\Delta\theta_{\text{tot}} - \Delta\theta_s) + K_{N1}(\Delta\theta_{\text{tot}} - \Delta\theta_s)^2, \tag{2a}$$

$$K_{N0} \equiv [(dM_{\text{tot}}/d\Delta\theta_{\text{tot}})]_{\Delta\theta_{\text{tot}}=\Delta\theta_s}, \tag{2b}$$

$$K_{N1} \equiv (1/2)[(d^2M_{\text{tot}}/d\Delta\theta_{\text{tot}}^2)]_{\Delta\theta_{\text{tot}}=\Delta\theta_s}. \tag{2c}$$

Now, defining the dynamic moment to be the total minus the static moment and similarly for the jump in slope, the nonlinear dynamic representation of the bending spring is obtained as

$$M = K_{N0}\Delta\theta + K_{N1}\Delta\theta^2, \tag{3}$$

where K_{N0} and K_{N1} are defined above and M and $\Delta\theta$ (without subscripts) are the dynamic moment and jump in slope.

2.1. *Beam equation of motion and boundary conditions.* The equation of motion for an Euler–Bernoulli beam is

$$EI\frac{\partial^4 v}{\partial x^4} + \rho A\frac{\partial^2 v}{\partial t^2} = 0, \tag{4}$$

where EI is the flexural rigidity, ρ is the density, A is the cross-sectional area, $v(x,t)$ is the displacement of the mid-plane, defined positive in the upward direction, and $\theta(x,t) = (\partial v/\partial x)$ is the slope, defined positive in the counter-clockwise direction. The bending moment and shear force are $M(x,t) = EI(\partial^2 v/\partial x^2)$ and $Q(x,t) = EI(\partial^3 v/\partial x^3)$. (See [Mokashi and Mendelsohn 2008, Figure 1] for sign conventions.) The following boundary conditions can be specified for all times $t > 0$. At the simple supports ($x = 0, L$) the displacement and rotational moment are zero. Since the length of the line-spring is always zero, static equilibrium requires that the bending moment and shear force across the crack plane be continuous.

$$\frac{\partial^2 v}{\partial x^2}(c-, t) = \frac{\partial^2 v}{\partial x^2}(c+, t), \tag{5}$$

$$\frac{\partial^3 v}{\partial x^3}(c-, t) = \frac{\partial^3 v}{\partial x^3}(c+, t). \tag{6}$$

where $c-$ and $c+$ indicate limits from the left and right, respectively as x goes to c. The jump in displacement and slope, respectively, across the crack plane are defined as

$$\Delta v(t) \equiv v(c+, t) - v(c-, t), \tag{7}$$

$$\Delta\theta(t) \equiv \frac{\partial v}{\partial x}(c+, t) - \frac{\partial v}{\partial x}(c-, t). \tag{8}$$

The bending moment is related to the change in slope across the crack plane through the nonlinear bending relation (3):

$$M = EI \frac{\partial^2 v}{\partial x^2}(c-, t) = K_{N0} \, \Delta\theta(t) + K_{N1} \, (\Delta\theta(t))^2. \tag{9}$$

The shear spring relation is, however, linear:

$$Q = EI(\partial^3 v/\partial x^3) = -K_{T0} \, \Delta v(t). \tag{10}$$

2.2. Nondimensionalization and perturbed boundary conditions.

In the following perturbation analysis, the zeroth order solution will be eigenfunctions of the linear free-vibration problem, involving K_{N0} and K_{T0} only. These eigenfunctions will be determined in terms of a free amplitude constant, say, A_0, which is assumed to be small compared to the length of the beam. Write the deflection $v(x, t)$ in a variable separable form in the two solution regions: L to the left of crack plane ($0 < \bar{x} < \bar{c}$) and R to the right of the crack plane ($\bar{c} < \bar{x} < \bar{L}$), where $\bar{x} \equiv x/L$. The deflections in the left and right regions are then

$$v(x, t) = v_L(x, t) = A_0 \, \phi_L(\bar{x}) \, T(t), 0 < \bar{x} < \bar{c}, \tag{11}$$

$$v(x, t) = v_R(x, t) = A_0 \, \phi_R(\bar{x}) \, T(t), \bar{c} < \bar{x} < \bar{L}. \tag{12}$$

A is a free parameter representing the vibration amplitude. Substituting this notation into the linear dimensional boundary conditions (5), (6), (9) and (10) yields

$$\phi_L''(\bar{c}) = \phi_R''(\bar{c}) \tag{13}$$

$$\phi_L'''(\bar{c}) = \phi_R'''(\bar{c}) \tag{14}$$

$$\phi_L''(\bar{c})T(t) = \bar{K}_{N0}[\Delta\phi' T(t) + \epsilon_N (\Delta\phi'^2)T^2(t)], \tag{15}$$

$$\phi_L'''(\bar{c}) = -\bar{K}_{T0}\Delta\phi, \tag{16}$$

where $' \equiv (d/d\bar{x}) = L(\partial/\partial x)$, and

$$\bar{K}_{T0} \equiv (K_{T0} \, L^3/EI), \tag{17}$$

$$\Delta\phi = \phi_R(\bar{c}) - \phi_L(\bar{c}), \tag{18}$$

$$\bar{K}_{N0} \equiv (K_{N0} \, L/EI), \tag{19}$$

$$\epsilon_N \equiv (K_{N1}/K_{N0})(A_0/L), \tag{20}$$

$$\Delta\phi' \equiv \phi_R'(\bar{c}) - \phi_L'(\bar{c}). \tag{21}$$

The parameters, $\bar{K}_{N0}$, $\bar{K}_{T0}$ and ϵ_N are dimensionless and ϵ_N is assumed to be a small quantity, which is easily achieved by keeping the vibration amplitude A_0 several orders of magnitude smaller than the beam length. The deflection of the beam in the left and right regions are now expanded in powers of ϵ_N.

$$v(x, t) = v_L(x, t) = A_0 \, [\phi_{L0}(\bar{x}) \, T_0(t) + \epsilon_N \, \phi_{L1}(\bar{x}) \, T_1(t) + ...], \; 0 < \bar{x} < \bar{c},$$
$$v(x, t) = v_R(x, t) = A_0 \, [\phi_{R0}(\bar{x}) \, T_0(t) + \epsilon_N \, \phi_{R1}(\bar{x}) \, T_1(t) + ...], \; \bar{c} < \bar{x} < \bar{L}. \tag{22}$$

The solution forms obtained in (22) are substituted in (15) to get the following expression for the nonlinear boundary condition

$$\phi_{L0}''(\bar{c})\, T_0(t) \,+\, \epsilon_N\, \phi_{L1}''(\bar{c})\, T_1(t)$$
$$= \bar{K}_{N0}\, [\Delta\phi_0'\, T_0(t) + \epsilon_N\, \Delta\phi_1'\, T_1(t) + ... \,\epsilon_N\, (\Delta\phi_0'\, T_0(t) + \epsilon_N\, \Delta\phi_1'\, T_1(t) + ...)^2]. \quad (23)$$

Keeping only the zeroth and first-order terms of ϵ_N, this can be rewritten as

$$\phi_{L0}''(\bar{c})\, T_0(t) \,+\, \epsilon_N\, \phi_{L1}''(\bar{c})\, T_1(t) = \bar{K}_{N0}\, [\Delta\phi_0'\, T_0(t) + \epsilon_N\, (\Delta\phi_1'\, T_1(t) + (\Delta\phi_0')^2\, T_0^2(t))]. \quad (24)$$

In order that (22) be satisfied for all times t, we must have $T_1(t) = T_0^2(T)$. The solution forms for $v(x, t)$ in (22) are now substituted into the linear nondimensional boundary conditions, (13)–(16). The resulting expressions and (24) are then separated into zeroth order and first-order contributions in ϵ_N, to obtain separate linear nondimensional, time-independent boundary conditions for the zeroth and the first-order problems.

The zeroth order crack plane boundary conditions are written as:

$$\begin{aligned}
\phi_{L0}''(\bar{c}) &= \phi_{R0}''(\bar{c}), \\
\phi_{L0}'''(\bar{c}) &= \phi_{R0}'''(\bar{c}), \\
\phi_{L0}''(\bar{c}) - \bar{K}_{N0}\, \Delta\phi_0' &= 0, \\
\phi_{L0}'''(\bar{c}) + \bar{K}_{T0}\, \Delta\phi_0 &= 0.
\end{aligned} \quad (25)$$

The first-order crack plane boundary conditions are written as:

$$\begin{aligned}
\phi_{L1}''(\bar{c}) &= \phi_{R1}''(\bar{c}), \\
\phi_{L1}'''(\bar{c}) &= \phi_{R1}'''(\bar{c}), \\
\phi_{L1}''(\bar{c}) - \bar{K}_{N0}\, \Delta\phi_1' &= \bar{K}_{N0}\, (\Delta\phi_0')^2, \\
\phi_{L1}'''(\bar{c}) + \bar{K}_{T0}\, \Delta\phi_1 &= 0.
\end{aligned} \quad (26)$$

Note that the time functions factor out of all of these linear boundary conditions if $T_1(t) = T_0^2(t)$. The zeroth and first-order jumps $\Delta\phi_0$, $\Delta\phi_0'$ and $\Delta\phi_1'$ are defined analogously to the total jumps in (18) and (21) by adding a subscript of 0 or 1.

3. Zeroth order solution

Assuming the time dependence $T_0(t) = \sin(\omega_0 t)$ and substituting the zeroth order contributions to the displacement forms in (22) into the equation of motion, (4), leads to the forms:

$$\begin{aligned}
v_{L0}(x, t) &= A_0\phi_{L0}(\bar{x})T_0(t) \\
&= A_0[C_1 \sin(\bar{k}_0\bar{x}) + C_2 \sin h(\bar{k}_0\bar{x})]\sin(\omega_0 t),
\end{aligned}$$

$$\begin{aligned}
v_{R0}(x, t) &= A_0\phi_{R0}(\bar{x})T_0(t) \\
&= A_0[C_3 \sin(\bar{k}_0\bar{x}) - \tan(\bar{k}_0)\cos(\bar{k}_0\bar{x})] + C_4[\sin h(\bar{k}_0\bar{x}) - \tan h(\bar{k}_0)\cos h(\bar{k}_0\bar{x})]\sin(\omega_0 t),
\end{aligned}$$

$$(27)$$

where $\bar{k}_0 \equiv k_0 L$ and the wave number k_0 and frequency ω_0 are related by

$$k_0^2 = \omega_0 \sqrt{(\rho A / E I)}. \tag{28}$$

The solution forms in Equation (27) satisfy the simple support boundary conditions of zero displacement and zero moment at $\bar{x} = 0$ and $\bar{x} = 1$. Using a linear system in the unknown constants the boundary conditions (25) can be written as

$$[A] \cdot (\mathbf{x}) = 0 \tag{29}$$

where $(\mathbf{x})$ is the vector consisting of the four constants C_1, C_2, C_3 and C_4 and $[A]$ is the coefficient matrix, shown below

$$\begin{bmatrix} -\sin(\bar{k}_0\bar{c}) & \sinh(\bar{k}_0\bar{c}) & \sin(\bar{k}_0\bar{c}) - \tan(\bar{k}_0)\cos(\bar{k}_0\bar{c}) & \tanh(\bar{k}_0)\cosh(\bar{k}_0\bar{c}) - \sinh(\bar{k}_0\bar{c}) \\ -\cos(\bar{k}_0\bar{c}) & \cosh(\bar{k}_0\bar{c}) & \cos(\bar{k}_0\bar{c}) + \tan(\bar{k}_0)\sin(\bar{k}_0\bar{c}) & \tanh(\bar{k}_0)\sinh(\bar{k}_0\bar{c}) - \cosh(\bar{k}_0\bar{c}) \\ \tilde{K}_{N0}\cos(\bar{k}_0\bar{c}) - \sin(\bar{k}_0\bar{c}) & \tilde{K}_{N0}\cosh(\bar{k}_0\bar{c}) + \sinh(\bar{k}_0\bar{c}) & -\tilde{K}_{N0}(\cos(\bar{k}_0\bar{c}) + \tan(\bar{k}_0)\sin(\bar{k}_0\bar{c})) & \tilde{K}_{N0}(\tanh(\bar{k}_0)\sinh(\bar{k}_0\bar{c}) - \cosh(\bar{k}_0\bar{c})) \\ \tilde{K}_{T0}\sin(\bar{k}_0\bar{c}) + \cos(\bar{k}_0\bar{c}) & \tilde{K}_{T0}\sinh(\bar{k}_0\bar{c}) - \cosh(\bar{k}_0\bar{c}) & \tilde{K}_{T0}(\tan(\bar{k}_0)\cos(\bar{k}_0\bar{c}) - \sin(\bar{k}_0\bar{c})) & \tilde{K}_{T0}(\tanh(\bar{k}_0)\cosh(\bar{k}_0\bar{c}) - \sinh(\bar{k}_0\bar{c})) \end{bmatrix}$$

The dimensionless bending and shear stiffnesses in $[A]$ are defined as

$$\tilde{K}_{N0} \equiv \frac{\bar{K}_{N0}}{\bar{k}_0} = \frac{K_{N0}}{E I k_0} = \frac{12}{E W^3 k_0}\left(\frac{K_{N0}}{b}\right), \tag{30}$$

$$\tilde{K}_{T0} \equiv \frac{\bar{K}_{T0}}{\bar{k}_0^3} = \frac{K_{T0}}{E I k_0^3} = \frac{12}{E W^3 k_0}\left(\frac{K_{T0}}{b}\right) \tag{31}$$

where W is the depth and b is the thickness of the beam. Setting the determinant of the matrix $[A]$ equal to zero for given crack position, $\bar{c}$ and stiffnesses $\tilde{K}_{NO}$ and $\tilde{K}_{TO}$ yields an infinite number of eigenvalues

$$k_{0n}; \quad n = 1, 2, 3, \ldots \tag{32}$$

For a given mode and k_{0n} the mode shapes can be determined by solving any three of the four equations of the linear system, (29), for any three of the constants (C_1, C_2, C_3, C_4) in terms of the fourth and substituting in (27).

4. First-order solution

For each of the infinite zeroth order modes with wavenumber k_{0n} and frequency ω_{0n} ($n = 1, 2, 3, \ldots$), there is a first order solution with wavenumber k_{1n} and frequency ω_{1n}. For convenience, the index n is suppressed throughout this section. Since there is already an undetermined amplitude constant A_0 in the zeroth order solution, (27), one of the four constants C_1, C_2, C_3, C_4 may be taken to be unity without loss of generality. Hence from here on, let $C_1 = 1$.

The first-order crack plane boundary conditions can be written time-independently (see Equation (26)) only if $T_1(t) = T_0^2(t)$. For the assumed $T_0(t) = \sin(\omega t)$ above

$$T_1(t) = T_0^2(t) = \sin^2(\omega_0 t) = 1/2 - 1/2\cos(2\omega_0 t) \cong -1/2\cos(2\omega_0 t), \tag{33}$$

where the last relation indicates the dynamic contribution to $T_1(t)$. Hence, for the first-order solution, the frequency is $\omega_1 = 2\omega_0$, and $k_1 = \sqrt{2}k_0$, (28). The first order solution for the deflections to the left

and right of the crack planes that satisfy the simple support conditions at $\bar{x} = 0$ and $\bar{x} = 1$ can thus be defined as

$$
\begin{aligned}
v_{L1}(x, t) &= \epsilon_N A_0 \phi_{L1}(\bar{x}) T_1(t) \\
&= \epsilon_N A_0 \left[D_1 \sin(\bar{k}_1 \bar{x}) + D_2 \sinh(\bar{k}_1 \bar{x}) \right] (-1/2 \cos(2\omega_0 t)),
\end{aligned}
$$

$$
\begin{aligned}
v_{R1}(x, t) &= \epsilon_N A_0 \phi_{L1}(\bar{x}) T_1(t) \\
&= \epsilon_N A_0 \left[D_3 \sin(\bar{k}_1 \bar{x}) - \tan(\bar{k}_1) \cos(\bar{k}_1 \bar{x}) \right] \\
&\qquad + D_4 \left[\sinh(\bar{k}_1 \bar{x}) - \tanh(\bar{k}_1) \cosh(\bar{k}_1 \bar{x}) \right] (-1/2 \cos(2\omega_0 t)),
\end{aligned}
\tag{34}
$$

where $\bar{k}_1 \equiv k_1 L$. The single higher harmonic is at twice the frequency and is phase shifted compared to the fundamental. Similar to the zeroth order, this deflection solution is now substituted in the first-order nondimensional, time-independent boundary conditions, (26), yielding the linear system

$$
[B] \cdot (\mathbf{y}) = (Z),
\tag{35}
$$

where $(\mathbf{y})$ is the vector consisting of the four constants D_1, D_2, D_3 and D_4, and the elements of (Z) are $Z_1 = 0$, $Z_2 = 0$, $Z_3 = 0$ and $Z_4 = (\tilde{K}_{N0} (\Delta\phi_0')^2 / 2\bar{k}_0)$. The term $\Delta\phi_0'$ in the fourth element of (Z) is obtained from the zeroth order mode shape as

$$
\Delta\phi_0' = \phi_{R0}'(\bar{c}) - \phi_{L0}'(\bar{c}).
\tag{36}
$$

The coefficient matrix $[B]$ is given below

$$
\begin{bmatrix}
-\sin(\bar{k}_1 \bar{c}) & \sinh(\bar{k}_1 \bar{c}) & \sin(\bar{k}_1 \bar{c}) - \tan(\bar{k}_1)\cos(\bar{k}_1 \bar{c}) & \tanh(\bar{k}_1)\cosh(\bar{k}_1 \bar{c}) - \sinh(\bar{k}_1 \bar{c}) \\
-\cos(\bar{k}_1 \bar{c}) & \cosh(\bar{k}_1 \bar{c}) & \cos(\bar{k}_1 \bar{c}) + \tan(\bar{k}_1)\sin(\bar{k}_1 \bar{c}) & \tanh(\bar{k}_1)\sinh(\bar{k}_1 \bar{c}) - \cosh(\bar{k}_1 \bar{c}) \\
\frac{\tilde{K}_{T0}}{2\sqrt{2}}\sin(\bar{k}_1 \bar{c}) + \cos(\bar{k}_1 \bar{c}) & \frac{\tilde{K}_{T0}}{2\sqrt{2}}\sinh(\bar{k}_1 \bar{c}) - \cosh(\bar{k}_1 \bar{c}) & \frac{\tilde{K}_{T0}}{2\sqrt{2}}[\tan(\bar{k}_1)\cos(\bar{k}_1 \bar{c}) - \sin(\bar{k}_1 \bar{c})] & \frac{\tilde{K}_{T0}}{2\sqrt{2}}[\tanh(\bar{k}_1)\cosh(\bar{k}_1 \bar{c}) - \sinh(\bar{k}_1 \bar{c})] \\
\frac{\tilde{K}_{N0}}{\sqrt{2}}\cos(\bar{k}_1 \bar{c}) - \sin(\bar{k}_1 \bar{c}) & \frac{\tilde{K}_{N0}}{\sqrt{2}}\cosh(\bar{k}_1 \bar{c}) + \sinh(\bar{k}_1 \bar{c}) & \frac{\tilde{K}_{N0}}{\sqrt{2}}[-\cos(\bar{k}_1 \bar{c}) - \tan(\bar{k}_1)\sin(\bar{k}_1 \bar{c}))] & \frac{\tilde{K}_{N0}}{\sqrt{2}}[\tanh(\bar{k}_1)\sinh(\bar{k}_1 \bar{c}) - \cosh(\bar{k}_1 \bar{c})]
\end{bmatrix}
$$

The nondimensional stiffnesses $\tilde{K}_{N0}$ and $\tilde{K}_{T0}$ are defined in Equation (30), substituting the solutions of (35) for D_1, D_2, D_3 and D_4 into (34) to get the first-order deflection of the beam.

5. Results

The length L and depth of the beam are taken to be 12.5 m and W 1.25 m, respectively. By appropriate scaling, results for any beam with a L/W ratio of 10 may be obtained. The thickness of the beam, b is not a critical parameter since most of the vibration parameters are independent of the thickness. The dimensionless crack ratio $\bar{a}$ is taken to be 0.34 for all results. The material of the beam is chosen as aluminum (Young's modulus $E = 72.8$ GPa, $\nu = 0.3$). Results for other $\bar{a}$ ratios and beam materials do not reveal any new patterns or insights. Since the even modes are antisymmetric about the midspan, the midspan is subjected only to shear and the even mode frequencies do not depend on the nonlinear bending stiffness.

The remaining parameters to prescribe and calculate are (K_{N0}/b), (K_{N1}/b) and (K_{T0}/b) which in turn will determine $\tilde{K}_{N0}$, $\tilde{K}_{T0}$ and ϵ_N in (30) and (20). For calculation purposes we note that the $\bar{M} - \Delta\theta$ curves from the BEM model [Mokashi and Mendelsohn 2008, Figures 8 and 9] really involve $\bar{M} \equiv M/b$ and are independent of b, the beam thickness. Hence we can approximate (K_{N0}/b) and (K_{N1}/b),

Equations (2b)–(2c), from the particular $\bar{M} - \Delta\theta$ curve using central differences. Similarly K_{T0}/b will be independent of b, and is calculated using the elastic analysis presented in [Yokoyama and Chen 1998]:

$$\frac{K_{T0}}{b} = \frac{E}{2\,(1-v^2)\int_0^{\bar{a}} \frac{F_T^2}{1-\bar{a}}\,d\bar{a}}, \tag{37}$$

where F_T is a function of the dimensionless crack ratio $\bar{a}$

$$F_T = 1.993\,\bar{a} + 4.513\,\bar{a}^2 - 9.516\,\bar{a}^3 + 4.482\,\bar{a}^4. \tag{38}$$

For the crack length $\bar{a} = 0.34$, the shear stiffness per unit thickness is calculated to be $\bar{K}_{T0}/b = 3.3986 \cdot 10^{11}\,N/m^2$. Finally the perturbation parameter ϵ_N, (20), is easily written in terms of K_{N1}/b and K_{N0}/b by dividing the numerator and denominator by b.

A typical set of results for the eigenvalues and zeroth and first order mode shapes are shown in Figures 3–5. Cohesive law 5 in [Mokashi and Mendelsohn 2008, Table 1] ($t_o = 50$ MPa, $\delta_o = 1.6$ mm) is used and the static preload per unit thickness is taken to be $\bar{M}_s = 7 \cdot 10^6$ N. From the data for the $M - \Delta\theta$ relation shown in [Mokashi and Mendelsohn 2008, Figure 9], the first and second derivatives are calculated using standard central differences as $K_{N0}/b = 8.4 \cdot 10^9$ N and $K_{N1}/b = 5.88 \cdot 10^{12}$ N and the free amplitude constant is taken to be $A_0 = 0.005\,m$, which gives a perturbation parameter value of $\epsilon_N = 0.28$. The first four wavenumbers and frequencies from the zeroth order eigenvalue problem are $k_{01} = 0.23883$, $k_{02} = 0.50248$, $k_{03} = 0.72195$, $k_{04} = 1.00389$, $\omega_{01} = 62.881$, $\omega_{02} = 278.337$, $\omega_{03} = 574.577$, $\omega_{04} = 1110.981$. Wave numbers are in m^{-1} and frequencies are in rad / sec. Figure 3 shows the zeroth order mode shapes and slope of the cracked beam with a cohesive zone for the lowest of these modes and compares them to the uncracked case. The presence of the crack causes an increase in maximum deflection and a jump in slope $\Delta\theta_o$ at the crack plane. Figure 4 shows the corresponding lowest mode first-order second harmonic solution for the deflection and slope for the cracked beam with a cohesive zone. The wavenumber and frequency are $k_{11} = 0.33776$ and $\omega_{11} = 125.762$. The magnitude of the first-order response depends on A_0^2, so it is quite sensitive to A_0, however the ratio of the first-order magnitudes to the zeroth order magnitudes depend only on A_0 through the perturbation parameter ϵ_N.
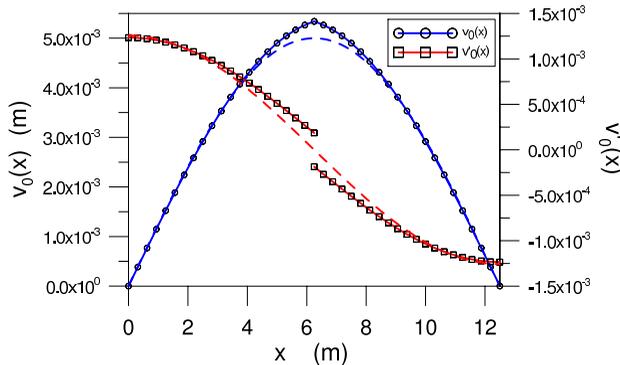
Figure 3. Zeroth-order mode shapes for deflection and slope. The solid curves are the uncracked mode shapes.
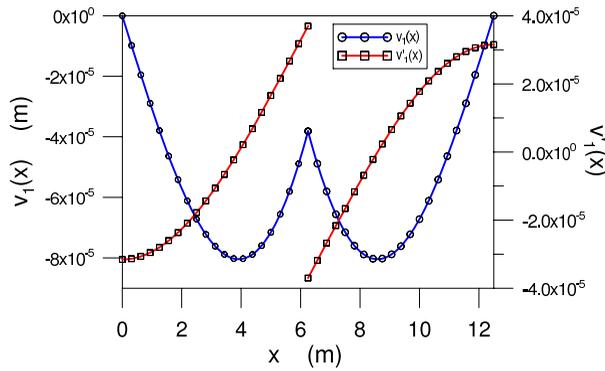
Figure 4. First-order mode shapes for deflection and slope.

The double hump in the first-order deflection appears as K_{N0} is reduced from a very large value representing an intact plane at $x = c$, and the cusp becomes deeper as K_{N0} is further reduced. The shapes of both v_1 and v_1' are independent of K_{N1} and ϵ_N. The jump in slope is distinctly observed and the maximum slopes occur at the crack plane rather than at the supports as in Figure 3. The magnitude of first-order jump in slope is observed to be on the order of 15% of the zeroth order jump in this example. Corresponding results for higher even modes show no effect of the crack or cohesive behavior and higher-order odd modes are similar to the plots shown in Figures 3 and 4, but with increasingly smaller magnitudes and wavelengths.

To study the effect of the cohesive law and its parameters, t_0 and δ_0 on the $\bar{M} - \Delta\theta$ relationship and the dynamic results, 11 cohesive laws were considered [Mokashi and Mendelsohn 2008, Table 1]. The
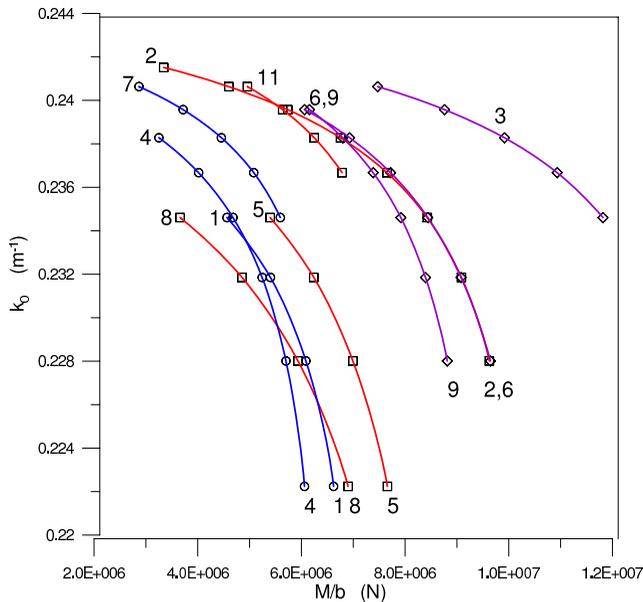
Figure 5. Variation of the first eigenvalue over applied moment.

amplitude of vibration A_0 is 0.001 in these results. All other parameters are as given above. Figure 5 shows the variation of the fundamental eigenvalue over applied static moment, $\bar{M}_s$ for all of the cohesive laws. It can be seen that eigenvalues drop with increasing moments, starting with a maximum eigenvalue of 0.243. This is lower than the first eigenvalue for an uncracked beam ($k_{01\text{uncracked}} \approx 0.25$). The variation in eigenvalues show some dependence on J_0, that is, with decreasing J_0, the eigenvalue decreases for a given moment. However, this dependence is not absolute, and some deviations are observed, as seen with cases 7 and 11 of [Mokashi and Mendelsohn 2008, Table 1]. The grouping by peak cohesive traction is only partially evident in these results, but the peak traction still has an influence.

The effect of the cohesive laws on the maximum modal amplitude is seen in Figure 7. When plotted against applied moment, $(v_0)_{\text{max}}$ shows a strong dependence on t_0. At any given moment, lower stresses lead to higher maximum modal amplitudes. For laws that share a common t_0, as the slope of the cohesive law becomes steeper J_o decreases, the cohesive law is exercised at a lower moment, and over the part of the load range the displacement increases with increasing slope of the law. This controls the branching off of, for example, the 6 and 9 curves from the 3 curve. The corresponding plots for $\Delta\theta$ are shown in Figure 8 and they are remarkably similar.

Next the ratios of the first-order responses to the zeroth order responses are plotted against applied moment. Figure 9 shows the maximum modal amplitude ratios (left) and the ratios of the jump in slopes for the first order to the zeroth order against applied moment (right). Both results show a strong dependence on J_0, that is, with decreasing J_0, higher ratios are obtained for a given moment. However, deviations to this trend are observed in cases 2, 8 and 11 [Mokashi and Mendelsohn 2008, Table 1].

A sensitivity study was done to understand the dependence of our dynamic model to the key parameters A_0, $\bar{K}_{N0}$ and $\bar{K}_{N1}$. Figure 6 (left) shows a plot of k_0, $(v_0)_{\text{max}}$ and $\Delta\theta_0$ against the zeroth order bending
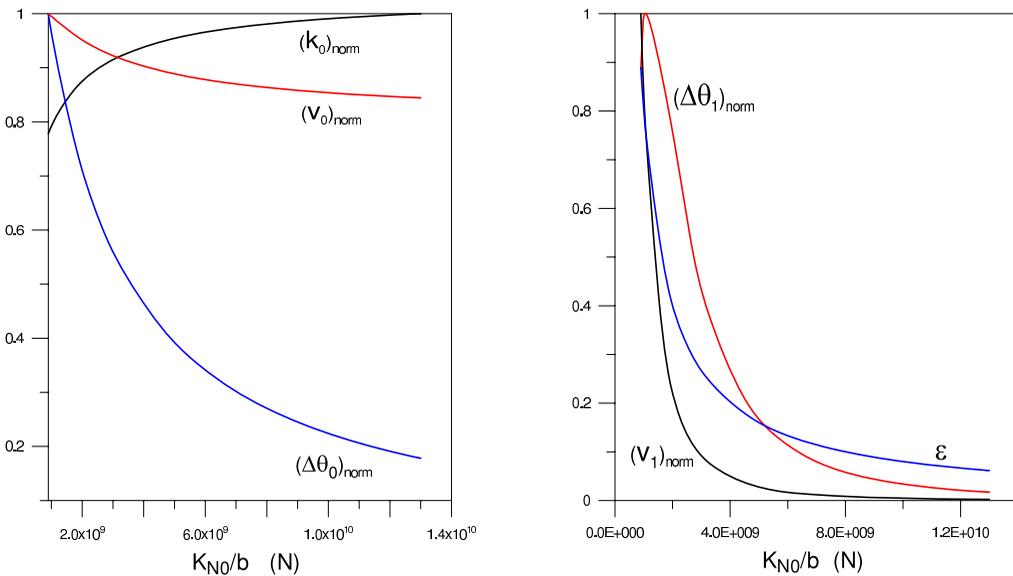
Figure 6. First eigenvalue: variation of k_0, $(v_0)_{\text{max}}$ and $\Delta\theta_0$ (left); variation of $(v_1)_{\text{max}}$ and $\Delta\theta_1$ and ϵ over bending stiffness (right). $A_0 = 0.01$.
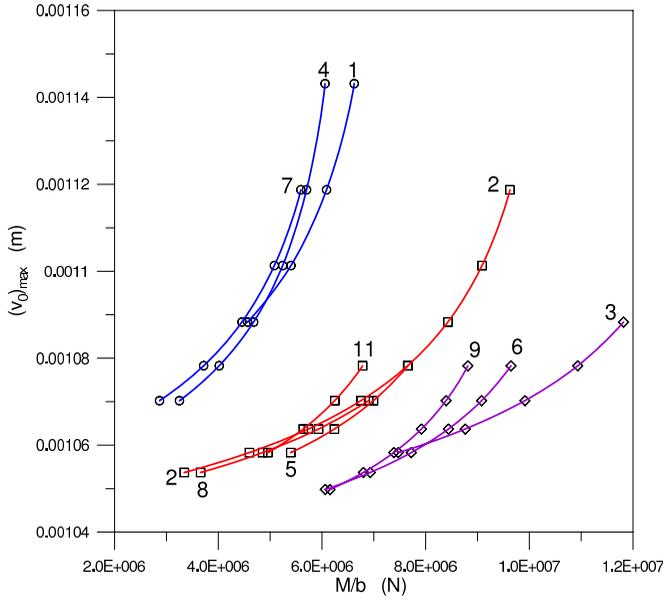
Figure 7. Variation of the maximum modal amplitude for the first eigenvalue over applied moment.

stiffness per unit thickness, $\bar{K}_{N0}$. The physical range of $\bar{K}_{N0}$ considered spans from very high compliance that approximates a plastic hinge on the lower end to high stiffness approximating an uncracked beam on the higher end. k_0 shows an increase with increasing bending stiffness, asymptotically approaching 0.25, which is the first eigenvalue for the uncracked beam. $(v_0)_{\max}$ and $\Delta\theta_0$, however, decrease with an
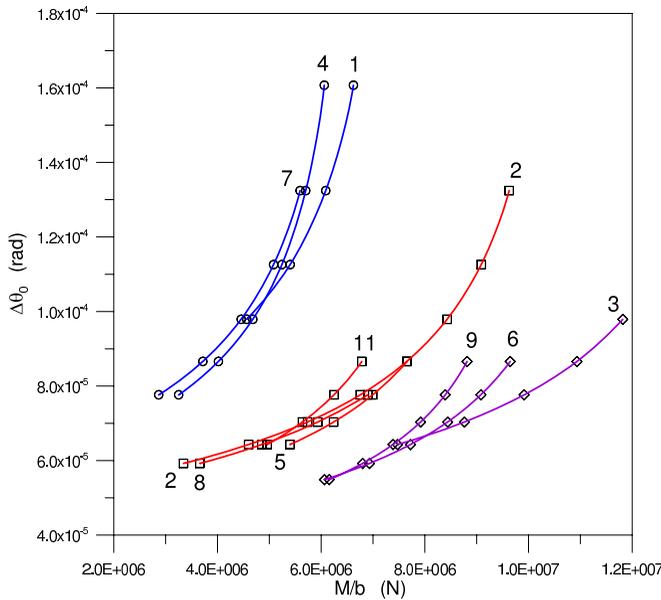
Figure 8. Variation of the jump in slope for the first eigenvalue over applied moment.
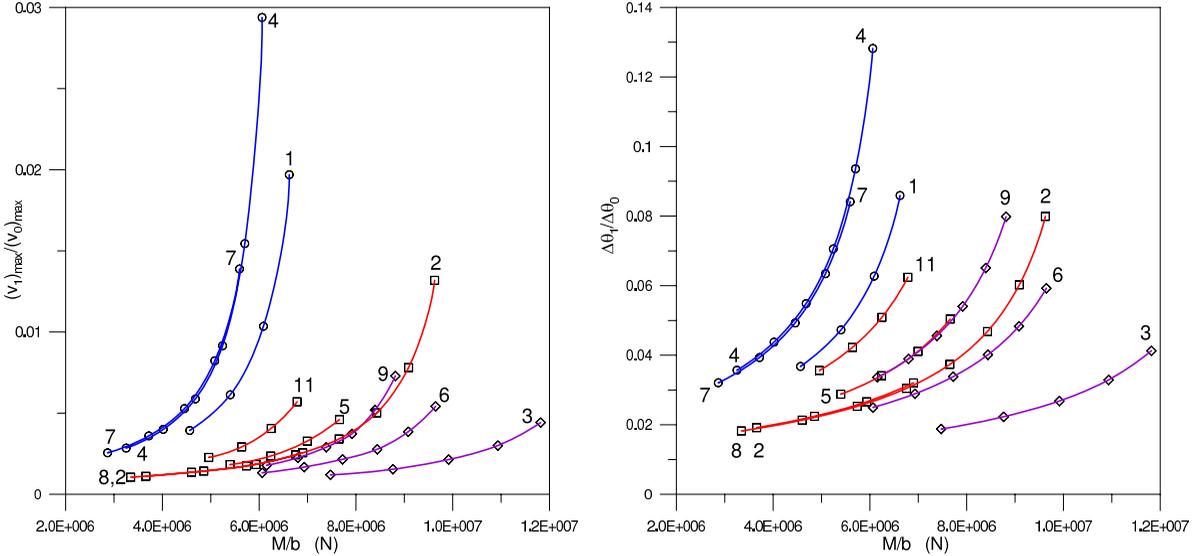
Figure 9. First eigenvalue: ratio of first- to zeroth-order maximum modal amplitude over applied moment (left); ratio of first- to zeroth-order jump in slope over applied moment (right).

increase in $\bar{K}_{N0}$, asymptotically reaching the uncracked condition. $(v_0)_{\max}$ and $\Delta\theta_0$ scale with A_0, that is, using different values of A_0, a family of similar curves can be obtained. A_0 is taken to be 0.01 in Figure 6 (left). Knowing $(v_0)_{\max}$ and $\Delta\theta_0$, it may then be possible to obtain both A_0 and the zeroth order bending stiffness, $\bar{K}_{N0}$. It is to be noted that k_0 does not depend on either A_0 or $\bar{K}_{N1}$, and both $(v_0)_{\max}$ and $\Delta\theta_0$ do not depend on $\bar{K}_{N1}$.

Figure 6 (right) shows a plot of $(v_1)_{\max}$, $\Delta\theta_1$ and ϵ_N against $\bar{K}_{N0}$. The first-order bending stiffness per unitthickness $\bar{K}_{N1}$ is taken to be $-1 \cdot 10^{12}$ N. All the three parameters show a sharp decrease with increasing stiffness. All of these parameters scale with the product $A_0 \cdot \bar{K}_{N1}$, that is, using different values of $A_0 \cdot \bar{K}_{N1}$, a family of similar curves can be obtained. Knowing A_0 and $\bar{K}_{N0}$ from the previous plots and $(v_1)_{\max}$ or $\Delta\theta_1$ from this plot, it may then be possible to obtain the $A_0 \cdot \bar{K}_{N1}$ term. Since A_0 is known, the first-order bending stiffness, $\bar{K}_{N1}$ could then be obtained. Results for the third eigenvalue are in [Vedachalam 2007] and show similar trends.

6. Conclusions

This paper addresses the issue of a linear softening cohesive zone ahead of a crack tip and its effect on the vibrational response of an edge-cracked beam. For a given crack length, presence of the cohesive zone leads to an additional reduction in the fundamental natural frequency, and induces nonlinearity leading to a second harmonic. The dynamic response is controlled by the critical yield stress, t_o or the critical fracture energy J_{Io}, much more than the crack tip opening displacement δ_o or the slope of the cohesive law. The state of damage affects the $\Delta\theta$ ratios more strongly than the modal amplitude ratios. $\Delta\theta$ ratios can, therefore, be used effectively in cohesive damage characterization. Within physical ranges of the dynamic spring constants, the first-order harmonic is observed to be quite significant when compared to

the fundamental. This model has potential for use in nondestructive cohesive material characterization in beam-like structures. There is potential for determining the dynamic spring constants from the dynamic responses. However, the relationship between the spring constants and the cohesive law parameters is less clear at this point and needs to be explored more in order to move towards an experimental inverse technique based on the present modeling.

References

[Bamnios and Trochidis 1995a] G. Bamnios and A. Trochidis, "Dynamic behaviour of a cracked cantilever beam", *Appl. Acoust.* **45**:2 (1995), 97–112.

[Bamnios and Trochidis 1995b] G. Bamnios and A. Trochidis, "Mechanical impedance of a cracked cantilever beam", *J. Acoust. Soc. Am.* **97**:6 (1995), 3625–3635.

[Brandon et al. 1999] J. A. Brandon, A. E. Stephens, E. M. O. Lopes, and A. S. K. Kwan, "Spectral indicators in structural damage identification: a case study", *Proc. Inst. Mech. Eng. C, J. Mech. Eng. Sci.* **213**:4 (1999), 411–415.

[Chondros 2001] T. G. Chondros, "The continuous crack flexibility model for crack identification", *Fatigue Fract. Eng. Mater. Struct.* **24**:10 (2001), 643–650.

[Chondros and Dimarogonas 1998] T. G. Chondros and A. D. Dimarogonas, "Vibration of a cracked cantilever beam", *J. Vib. Acoust.* (*ASME*) **120**:3 (1998), 742–746.

[Chondros et al. 1998] T. G. Chondros, A. D. Dimarogonas, and J. Yao, "A continuous cracked beam vibration theory", *J. Sound Vib.* **215**:1 (1998), 17–34.

[Chondros et al. 2001] T. G. Chondros, A. D. Dimarogonas, and J. Yao, "Vibration of a beam with a breathing crack", *J. Sound Vib.* **239**:1 (2001), 57–67.

[Dimarogonas 1996] A. D. Dimarogonas, "Vibrations of cracked structures: a state of the art review", *Eng. Fract. Mech.* **55**:5 (1996), 831–857.

[Gounaris and Papadopoulos 1997] G. D. Gounaris and C. A. Papadopoulos, "Analytical and experimental crack identification of beam structures in air or in fluid", *Comput. Struct.* **65**:5 (1997), 633–639.

[Gudmundson 1982] P. Gudmundson, "Eigenfrequency changes of structures due to cracks, notches or other geometrical changes", *J. Mech. Phys. Solids* **30**:5 (1982), 339–353.

[Gudmundson 1983] P. Gudmundson, "The dynamic behaviour of slender structures with cross-sectional cracks", *J. Mech. Phys. Solids* **31**:4 (1983), 329–345.

[Kessler et al. 2002] S. S. Kessler, S. M. Spearing, M. J. Atalla, C. E. S. Cesnik, and C. Soutis, "Damage detection in composite materials using frequency response methods", *Compos. B Eng.* **33**:1 (2002), 87–95.

[Li 2001] Q. S. Li, "Dynamic behavior of multistep cracked beams with varying cross section", *J. Acoust. Soc. Am.* **109**:6 (2001), 3072–3075.

[Mahmoud et al. 1999] M. A. Mahmoud, M. Abu Zaid, and S. Al Harashani, "Numerical frequency analysis of uniform beams with a transverse crack", *Commun. Numer. Methods Eng.* **15**:10 (1999), 709–715.

[Mendelsohn 2006] D. A. Mendelsohn, "Free vibration of an edge-cracked beam with a Dugdale–Barenblatt cohesive zone", *J. Sound Vib.* **292**:1–2 (2006), 59–81.

[Mokashi 2007] P. S. Mokashi, *Numerical modeling of homogeneous and bimaterial crack tip and interfacial cohesive zones with various traction-displacement laws*, Ph.D. thesis, The Ohio State University, 2007.

[Mokashi and Mendelsohn 2008] P. S. Mokashi and D. A. Mendelsohn, "Nonlinear vibration of an edge-cracked beam with a cohesive zone, I: Nonlinear bending load-displacement relations for a linear softening cohesive law", *J. Mech. Mater. Struct.* **3**:8 (2008), 1573–1588.

[Pecorari 2003] C. Pecorari, "Nonlinear interaction of plane ultrasonic waves with an interface between rough surfaces in contact", *J. Acoust. Soc. Am.* **113**:6 (2003), 3065–3072.

[Pecorari 2004] C. Pecorari, "Adhesion and nonlinear scattering by rough surfaces in contact: beyond the phenomenology of the Preisach–Mayergoyz framework", *J. Acoust. Soc. Am.* **116**:4 (2004), 1938–1947.

[Pecorari and Poznić 2005] C. Pecorari and M. Poznić, "Nonlinear acoustic scattering by a partially closed surface-breaking crack", *J. Acoust. Soc. Am.* **117**:2 (2005), 592–600.

[Rice and Levy 1972] J. R. Rice and N. Levy, "The part-through surface crack in an elastic plate", *J. Appl. Mech.* (*ASME*) **39** (1972), 185–194.

[Ruotolo et al. 1996] R. Ruotolo, C. Surace, P. Crespo, and D. Storer, "Harmonic analysis of the vibrations of a cantilevered beam with a closing crack", *Comput. Struct.* **61**:6 (1996), 1057–1074.

[Sekhar and Balaji Prasad 1998] A. S. Sekhar and P. Balaji Prasad, "Crack identification in a cantilever beam using coupled response measurements", *J. Eng. Gas Turb. Power* (*ASME*) **120**:4 (1998), 775–777.

[Shifrin and Ruotolo 1999] E. I. Shifrin and R. Ruotolo, "Natural frequencies of a beam with an arbitrary number of cracks", *J. Sound Vib.* **222**:3 (1999), 409–423.

[Vedachalam 2007] S. Vedachalam, *A perturbation approach to the nonlinear vibration of a cracked and cohesively damaged beam*, Master's thesis, The Ohio State University, 2007.

[Yokoyama and Chen 1998] T. Yokoyama and M.-C. Chen, "Vibration analysis of edge-cracked beams using a line-spring model", *Eng. Fract. Mech.* **59**:3 (1998), 403–409.

DANIEL A. MENDELSOHN: mendelsohn.1@osu.edu
Department of Mechanical Engineering, Scott Laboratory, The Ohio State University, 201 W. 19th Avenue, Columbus, OH 43210, United States

SRIDHAR VEDACHALAM: vedachalam.1@osu.edu
Environmental Science Graduate Program, The Ohio State University, 260 Ag. Engineering Building, 590 Woody Hayes Drive, Columbus, OH 43210 United States

CLAUDIO PECORARI: claudio.pecorari@afconsult.com
NDE System Development, AF-KONTROLL AB, Linkoping, Sweden, SE-582 22, Sweden

PRASAD S. MOKASHI: mokashi.1@osu.edu
Department of Mechanical Engineering, Scott Laboratory, The Ohio State University, 201 W. 19th Avenue, Columbus, Ohio 43210, United States